Results in Physics 10 (2018) 395–405

Contents lists available at ScienceDirect

Results in Physics

journal homepage: www.elsevier.com/locate/rinp

Analysis of heat transfer in nanofluid past a convectively heated permeable stretching/shrinking sheet with regression and stability analyses

Shah Jahan[a], Hamzah Sakidin[a], Roslinda Nazar[b,*], Ioan Pop[c]

[a] Fundamental and Applied Sciences Department, Universiti Teknologi PETRONAS, 32610 Bandar Seri Iskandar, Perak, Malaysia
[b] School of Mathematical Sciences, Faculty of Science & Technology, Universiti Kebangsaan Malaysia, 43600 UKM Bangi, Selangor, Malaysia
[c] Department of Mathematics, Babes-Bolyai University, R-400084 Cluj-Napoca, Romania

ARTICLE INFO

Keywords:
Convectively heated stretching/shrinking sheet
Passive control of nanoparticles
Numerical approach
Regression and stability analyses

ABSTRACT

In this article, we study the revised model of boundary-layer flow past a permeable stretching/shrinking sheet over the heated surface in a nanofluid with stability and regression analyses. The revised model refers to a physically more realistic approach, where the nanoparticle fraction can be controlled on the boundary in a similar way as for temperature on the boundary. The system of nonlinear similarity ordinary differential equations is solved numerically and dual solutions are found for both stretching and shrinking sheets up to a certain range of the stretching/shrinking parameter. Effect of pertinent parameters on the skin friction coefficient, the local Nusselt number, the velocity, temperature and concentration profiles are deliberated. Stability analysis is executed to know about the stability of dual solutions when sheet is being stretched or shrunk under the suction effect. The local Nusselt number is estimated through regressions for both stretching and shrinking sheets. It is observed through regressions and graphical results that the Brownian motion has no more effect on the heat transfer rate. The Schmidt number gives a very minimal effect on the heat transfer rate, while with an increase in Biot number, the heat transfer rate increases but at a higher value of Biot number accomplishes a constant wall temperature condition. The Brownian and thermophoresis parameters should be kept small as mainly the transfer of heat is due to fluid motion. From the stability analysis, it is found through numeric values and graphical results that the first solution is stable and thus physically realizable. Finally, the flow pattern is analyzed, and it is observed that streamline contracts with the increase of the suction parameter.

Introduction

The convective heat transfer in nanofluid has a contemporary attention, and various researchers tried to make large improvement in convective heat transfer coefficient [1–7]. Buongiorno [8] evaluated different theories explaining the enhanced heat transfer characteristics of nanofluids and developed analytical model for convective transport in nanofluids which taken into account the Brownian diffusion and thermophoresis. On the other hand, boundary layer flows driven by stretching/shrinking sheet have numerous applications such as in cooling of continuous strips, wire drawing, producing glassware and crystal, drawing of paper film, capillary effect on very small pores, and others. As shrinking sheet flow is quite distinct from the stretching sheet, so suction effect has also been considered on stretching/shrinking sheet as it delays the boundary layer separation and makes the flow more stable. In view of that, various studies of the flow and heat transfer on stretching/shrinking sheet with different physical parameters have been investigated due to increasing engineering applications.

Khan and Pop [8] examined the boundary layer flow of nanofluid past a stretching sheet with constant surface temperature, then Makinde and Aziz [9] considered it with general form as convective boundary condition. Recently, Turkyilmazoglu [10] found the exact solution for some nanoliquid flow past a porous shrinking/stretching surfaces. It was reported that rate of heat transfer is highly dependent on the density of considered nanofluid and heat capacitance. Most recently Khan et al. [11] analytically examined the time dependent mixed convection effect in a couple stress nanofluid using an oscillatory stretching sheet and reported an enhancement in temperature distribution for Brownian and Hartman number. Furthermore, details on the convective heat transfer in nanofluid and relevant references on nanofluids can be found in the books by Das et al. [12], Vafai [13], Michaelides [14], Nield and Bejan [15], and Shenoy et al. [16], and in the review papers by Buongiorno et al. [17], Kakaç and Pramuanjaroenkij [18], Wong and Leon [19], Manca et al. [20], Mahian et al. [21], Sheikholeslami and Ganji [22], etc. These reviews discuss in detail the

* Corresponding author.
E-mail address: rmn@ukm.edu.my (R. Nazar).

https://doi.org/10.1016/j.rinp.2018.06.021
Received 14 April 2018; Received in revised form 27 May 2018; Accepted 10 June 2018
Available online 21 June 2018

preparation of nanofluids, theoretical and experimental investigations of thermal conductivity and viscosity of nanofluids, and the work done on convective transport in nanofluids. Recently, Ganvir et al. [23] made a review to analyze the characteristics of heat transfer in nanofluid and reported that enhancement in heat transfer is higher for metallic nanoparticles while thermal conductivity mechanism in term of enhancement is still not very clear. Most recently, Bahiraei et al. [24] gave a detail review about the recent publications dealing with heat transfer in nanofluids. It was mentioned, among other important issues that the accurate correlations, for the estimation/prediction of the pressure drop and heat transfer coefficient of nanofluids in heat exchangers, is very important. In addition, it is to be noted that nanofluids find significant importance in areas such as electronic cooling, vehicle cooling transformer, coolant cooling of electronic equipments, geophysical flows, aqueous solution-based crystal growth processes, etc. (see Rao and Srivastava [25]). Thus the accurate knowledge of thermal performance of nanofluids is of utmost importance.

Several researchers tried to enhance the heat transfer in a nanofluid with various physical aspects while using Buongiorno model [26]. But they always tried to control the nanoparticle concentration on the surface actively. This deficiency was first time removed by Kuznetsov and Nield [27] properly by passive control of nanoparticle fraction on the boundary and replaced the boundary conditions by a new physically more realistic set and thus termed it as “revised model”. Then they revised their different models using the same approach for different physical aspects [28–30]. In their studies, they controlled the nanoparticle fraction on the surface passively rather than actively and found that the heat transfer rate was independent of the Brownian motion parameter due to zero nanoparticle flux on the boundary. It means the contribution of Brownian motion to thermal energy equation tends to zero.

In other studies, researchers used this technique to control their nanoparticle fraction passively. Yadav et al. [31] reinvestigated the model for thermal instability in rotating nanofluid layer and reported that zero-flux boundary condition has a more destabilizing effect than constant boundary condition for alumina-water nanofluid, whereas reverse result seen for copper-water nanofluid. Again Yadav et al. [32] revised the model by considering zero nanoparticle flux on the surface for the onset of double diffusive nanofluid convection in a rotating porous medium, while Rana and Chand [33] reinvestigated the double diffusive convection of Rivlin-Ericksen nanofluid model and reported that oscillatory did not exist as R_n remains positive. Recently Jahan et al. [34] revised the nanofluid model over the moving surface in a flowing fluid by considering the zero flux on the boundaries. Most recently Uddin et al. [35] used a zero flux condition while studying the buoyancy effect on nanoliquid stagnation point flow over a convectively heated stretching sheet in the presence of magnetohydrodynamic (MHD).

Regarding the findings of multiple solutions, many researchers tried to find dual solutions, for example [36,37] but the majority of them did not explain about the stability of the outcoming solutions. It seems that Merkin [38] first time found the smallest eigenvalues for dual solutions and reported that positive eigenvalues were more stable as compared to negative eigenvalues. Later on, Weidman et al. [39] established a stability analysis by following Merkin [40] and found positive smallest eigenvalues for the first solutions and smallest negative eigenvalues for the second solutions and concluded that the first solution was stable, whereas the second solution was unstable. Few researchers have attempted the stability analysis successfully by following Weidman et al. [39] and Merkin [38]. For example, Merrill et al. [40] performed stability analysis for stagnation point flow, while Harris et al. [41] found that the first solution was stable through stability analysis. Rosca and Pop [42] performed the analysis for a vertical permeable stretching shrinking sheet. Ishak [43], Nazar et al. [44] and Hamid et al. [45] tested the stability of their solutions through stability analysis. Most recently, Awaludin et al. [46] and Rosca and Pop [47] implemented the stability analysis for the stagnation point flow and axisymmetric rotational stagnation point flow, respectively.

Based on the above studies, our aim is to reinvestigate the boundary-layer flow of a nanofluid past a stretching sheet over a heated surface by extending it to a permeable stretching/shrinking sheet with passive control of nanoparticle fraction on the boundary (see Makinde and Aziz [9]). Hence, nanoparticle fraction on the surface is adjusted accordingly. A major limitation of the paper by Makinde and Aziz [9] is to control fraction actively on the surface. Basically, to fix the nanoparticle concentration at the boundary is an arbitrary condition [48] and controlling the particle fraction on the wall will be difficult in practice. So it is required to use the more realistic condition, so that it can be controlled at the boundary in a similar direction as the temperature can be regulated. So we followed the studies mentioned above and used a more realistic approach to get better understanding about the heat transfer in nanofluids. Further, we found dual solutions and established the stability analysis for both solutions using bvp4c function. Regression analysis is carried out for the reduced Nusselt number. The effects of numerous flow parameters are examined for the skin friction coefficient, the local Nusselt number and some sample graphs of velocity, temperature and concentration profiles, respectively. Lastly, the flow pattern is observed by drawing streamlines for both solutions, and in all graphs, dotted lines represent the second solution, whereas solid line is the first solution.

Problem formulation

Consider a two-dimensional steady flow of a nanofluid past a permeable stretching/shrinking sheet. We assume that velocity of stretching/shrinking sheet is $u_w = bx$, b is constant, and it varies linearly from origin when $y = 0$ as shown in Fig. 1.

We consider the nanofluid in the region $y > 0$ and assume that surface sheet is heated due to convection from a hot fluid with temperature T_f and heat transfer coefficient h. C_w and C_∞ are the nanoparticle volume fractions on the wall and away from the wall when y has large values. Following Buongiorno's [26] model, we have the following equations:

$$\frac{\partial u}{\partial x} + \frac{\partial v}{\partial y} = 0, \tag{1}$$

$$u\frac{\partial u}{\partial x} + v\frac{\partial u}{\partial y} = -\frac{1}{\rho_f}\frac{\partial p}{\partial x} + \nu\left(\frac{\partial^2 u}{\partial x^2} + \frac{\partial^2 u}{\partial y^2}\right), \tag{2}$$

$$u\frac{\partial v}{\partial x} + v\frac{\partial v}{\partial y} = -\frac{1}{\rho_f}\frac{\partial p}{\partial y} + \nu\left(\frac{\partial^2 v}{\partial x^2} + \frac{\partial^2 v}{\partial y^2}\right), \tag{3}$$

$$u\frac{\partial T}{\partial x} + v\frac{\partial T}{\partial y} = \alpha\left(\frac{\partial^2 T}{\partial x^2} + \frac{\partial^2 T}{\partial y^2}\right) + \xi\left[D_B\left(\frac{\partial C}{\partial x}\frac{\partial T}{\partial x} + \frac{\partial C}{\partial y}\frac{\partial T}{\partial y}\right) + \frac{D_T}{T_\infty}\left\{\left(\frac{\partial T}{\partial x}\right)^2 + \left(\frac{\partial T}{\partial y}\right)^2\right\}\right], \tag{4}$$

$$u\frac{\partial C}{\partial x} + v\frac{\partial C}{\partial y} = D_B\left(\frac{\partial^2 C}{\partial x^2} + \frac{\partial^2 C}{\partial y^2}\right) + \left(\frac{D_T}{T_\infty}\right)\left(\frac{\partial^2 T}{\partial x^2} + \frac{\partial^2 T}{\partial y^2}\right) \tag{5}$$

Here u and v are velocity components in the respective directions, ν the kinematic viscosity, α the thermal diffusivity, $\xi = (\rho c)_p/(\rho c)_f$, D_B and D_T belong to the Brownian diffusion and thermophoretic diffusion coefficient, respectively. Following [27], the boundary conditions are as follows:

$$v = v_0,\ u = \lambda u_w,\ -k\frac{\partial T}{\partial y} = h(T_f - T),$$
$$D_B\frac{\partial C}{\partial y} + \frac{D_T}{T_\infty}\frac{\partial T}{\partial y} = 0 \quad \text{at } y = 0 \tag{6}$$

$$u \to 0,\ v \to 0,\ T \to T_\infty,\ C \to C_\infty \quad \text{as } y \to \infty, \tag{7}$$

where λ is the stretching/shrinking velocity with $\lambda > 0$ for stretching and $\lambda < 0$ for the shrinking case. v_0 belongs to the mass flux velocity

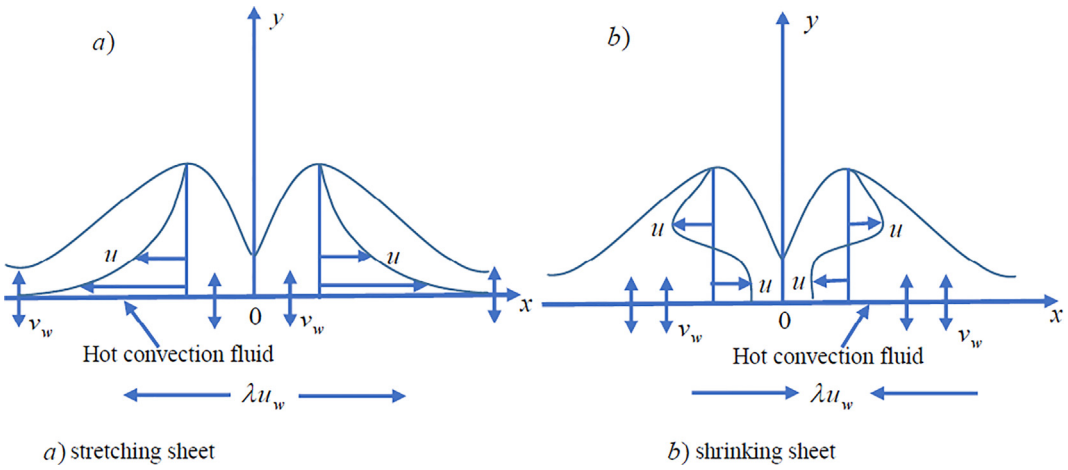

Fig. 1. Physical model and coordinate system.

and when $v_0 > 0$ for injection and $v_0 < 0$ is for suction. It is worth mentioning that in the previous model [9], they engaged the condition on the surface as $C = C_w$. A major limitation of this condition is to control the nanoparticle fraction actively. Here we have imposed zero flux condition. Further, we introduce the following transformations:

$$\psi = (b\nu)^{1/2} x f(\eta), \quad \theta(\eta) = \frac{T - T_\infty}{T_f - T_\infty}, \quad \phi(\eta) = \frac{C - C_\infty}{C_\infty},$$
$$\eta = (b/\nu)^{1/2} y, \tag{8}$$

The continuity equation is identically satisfied. The scale analysis of momentum equation in a direction normal to the sheet with the help of boundary layer approximation gives us

$$u \gg v \quad \text{so} \quad \frac{\partial u}{\partial y} \gg \frac{\partial u}{\partial x}, \frac{\partial v}{\partial x}, \frac{\partial v}{\partial y}, \Rightarrow \frac{\partial p}{\partial y} = 0.$$

Using Eq. (8) into Eqs. (2)–(7), we get the following nonlinear differential equations with boundary conditions:

$$f''' + ff'' - f'^2 = 0, \tag{9}$$

$$\frac{1}{\Pr}\theta'' + f\theta' + Nb\theta'\phi' + Nt(\theta')^2 = 0, \tag{10}$$

$$\phi'' + Sc\, f\phi' + \frac{Nt}{Nb}\theta'' = 0 \tag{11}$$

$$\left.\begin{aligned} &f(0) = S, \quad f'(0) = \lambda, \quad \theta'(0) = -Bi[1 - \theta(0)], \\ &Nb\phi'(0) + Nt\theta'(0) = 0 \\ &f'(\eta) \to 0, \quad \theta(\eta) \to 0, \quad \phi(\eta) \to 0 \quad as\ \eta \to \infty. \end{aligned}\right\} \tag{12}$$

where primes indicate differentiation with respect to η. Pr is the Prandtl number, Sc the Schmidt number, S the suction/injection parameter, Nb the Brownian motion parameter and Nt the thermophoresis parameter that are defined as:

$$\Pr = \nu/\alpha, \quad Sc = \nu/D_B, \quad S = -v_0/\sqrt{b\nu}$$
$$Nb = \frac{\xi D_B (C_\infty)}{\nu}, \quad Nt = \frac{\xi D_T (T_f - T_\infty)}{\nu T_\infty}, \quad Bi = \frac{h(\nu/\alpha)^{1/2}}{k} \tag{13}$$

The quantities of physical interests are the skin friction coefficient, and the local Nusselt number which are defined as

$$C_f = \frac{x\tau_w}{\rho u_w^2}, \quad Nu_x = \frac{xq_w}{k(T_f - T_\infty)} \tag{14}$$

where τ_w is the surface shear stress and q_w is the heat flux at the surface and both are defined as

$$\tau_w = \mu\left(\frac{\partial u}{\partial y}\right)_{y=0}, \quad q_w = -k\left(\frac{\partial T}{\partial y}\right)_{y=0} \tag{15}$$

Substituting (8) into (15) and using (14) we get as follow:

$$\mathrm{Re}_x^{1/2} C_f = f''(0), \quad \mathrm{Re}_x^{-1/2} Nu_x = -\theta'(0) \tag{16}$$

Here $\mathrm{Re}_x = \frac{u_w x}{\nu}$ represents the local Reynolds number. It is worth mentioning that now the mass flux is zero due to the new approach as mentioned in [27,30]. Following [49], an exact solution for Eq. (9) is

$$f(\eta) = S - \frac{2}{S \pm (S^2-4)^{1/2}} + \frac{2}{S \pm (S^2-4)^{1/2}} \exp^{\frac{S \pm (S^2-4)^{1/2}}{2}\eta} \tag{17}$$

It shows that we can get the second solution for $S > 2$ and it can be confirmed from the Fig. 4 that has been drawn for $f''(0)$ against S in this paper.

Hence, nanofluid momentum Eqs. (2) and (3) are identical to the momentum equation for pure fluid but here we are dealing with nanofluid, so viscosity (μ) strongly depends on the volume fraction of the nanoparticles. Turkyilmazoglu [50] has shown a link created between deforming surfaces phenomena considered in various geometries. Since we are dealing with linear sheet so when $n = 1$ and magnetic field, $\gamma = 0$, Eq. (4) in Turkyilmazoglu [50] becomes similar with Eq. (9) of our problem. Further, since all conservation Eqs. (2)–(5) are strongly coupled so following Turkyilmazoglu [50], we may conclude that the interchangeable role of mechanisms between stretching and shrinking sheets is present.

Stability analysis

Since there exist more than one solution of physical problem against single parameter, so it is important to find out the physical reliability of multiple solutions. The outcoming results from stability analysis could be engaged in engineering applications. In this respect, the stability of the dual solutions is investigated here. We introduce the new variable $\tau = bt$ that is associated with the initial value problem and is consistent with the question of which solution will be obtained in practice (stable and physically realizable). So we rewrite the Eqs. (2)–(5) and (8) as the following (see Merkin [38] and Weidman et al. [39]):

$$\psi = (b\nu)^{1/2} x f(\eta, \tau), \quad \theta(\eta, \tau) = \frac{T - T_\infty}{T_f - T_\infty}, \quad \phi(\eta, \tau) = \frac{C - C_\infty}{C_\infty},$$
$$\eta = (b/\nu)^{1/2} y, \quad \tau = bt \tag{18}$$

$$\frac{\partial u}{\partial t} + u\frac{\partial u}{\partial x} + v\frac{\partial u}{\partial y} = -\frac{1}{\rho_f}\frac{\partial p}{\partial x} + \nu\left(\frac{\partial^2 u}{\partial x^2} + \frac{\partial^2 u}{\partial y^2}\right), \tag{19}$$

$$\frac{\partial v}{\partial t} + u\frac{\partial v}{\partial x} + v\frac{\partial v}{\partial y} = -\frac{1}{\rho_f}\frac{\partial p}{\partial y} + \nu\left(\frac{\partial^2 v}{\partial x^2} + \frac{\partial^2 v}{\partial y^2}\right), \tag{20}$$

$$\frac{\partial T}{\partial t} + u\frac{\partial T}{\partial x} + v\frac{\partial T}{\partial y} = \alpha\left(\frac{\partial^2 T}{\partial x^2} + \frac{\partial^2 T}{\partial y^2}\right) + \xi\left[D_B\left(\frac{\partial C}{\partial x}\frac{\partial T}{\partial x} + \frac{\partial C}{\partial y}\frac{\partial T}{\partial y}\right) + \frac{D_T}{T_\infty}\left\{\left(\frac{\partial T}{\partial x}\right)^2 + \left(\frac{\partial T}{\partial y}\right)^2\right\}\right], \tag{21}$$

$$\frac{\partial C}{\partial t} + u\frac{\partial C}{\partial x} + v\frac{\partial C}{\partial y} = D_B\left(\frac{\partial^2 C}{\partial x^2} + \frac{\partial^2 C}{\partial y^2}\right) + \left(\frac{D_T}{T_\infty}\right)\left(\frac{\partial^2 T}{\partial x^2} + \frac{\partial^2 T}{\partial y^2}\right) \tag{22}$$

Using (18) into (19)–(22), we get the following equations:

$$\frac{\partial^3 f}{\partial \eta^3} + f\frac{\partial^2 f}{\partial \eta^2} - \left(\frac{\partial f}{\partial \eta}\right)^2 - \frac{\partial^2 f}{\partial \eta \partial \tau} = 0 \tag{23}$$

$$\frac{1}{\mathrm{Pr}}\frac{\partial^2 \theta}{\partial \eta^2} + f\frac{\partial \theta}{\partial \eta} + Nb\left(\frac{\partial \theta}{\partial \eta}.\frac{\partial \phi}{\partial \eta}\right) + Nt\left(\frac{\partial \theta}{\partial \eta}\right)^2 - \frac{\partial \theta}{\partial \tau} = 0 \tag{24}$$

$$\frac{\partial^2 \phi}{\partial \eta^2} + Sc\, f\frac{\partial \phi}{\partial \eta} + \frac{Nt}{Nb}\frac{\partial^2 \theta}{\partial \eta^2} - Sc\frac{\partial \phi}{\partial \tau} = 0 \tag{25}$$

subject to the boundary conditions

$$\left.\begin{aligned} &f(0,\tau) = S, \quad \tfrac{\partial f(0,\tau)}{\partial \eta} = \lambda, \quad \tfrac{\partial \theta(0,\tau)}{\partial \eta} = -Bi[1-\theta(0,\tau)], \\ &Nb\tfrac{\partial \phi(0,\tau)}{\partial \eta} + Nt\tfrac{\partial \theta(0,\tau)}{\partial \eta} = 0 \quad \text{at } y = 0 \\ &\tfrac{\partial f(\eta,\tau)}{\partial \eta} \to 0, \quad \theta(\eta,\tau) \to 0, \quad \phi(\eta,\tau) \to 0 \quad as\ \eta \to \infty. \end{aligned}\right\} \tag{26}$$

To check the stability of the steady flow solutions $f(\eta) = f_0(\eta)$, $\theta(\eta) = \theta_0(\eta)$, $\phi(\eta) = \phi_0(\eta)$ of Eqs. (9)–(11) satisfying the basic model by introducing the following terms (Merrill et al. [40], Weidman and Sprague [51]):

$$\begin{aligned} &f(\eta,\tau) = f_0(\eta) + e^{-\gamma\tau}F(\eta), \quad \theta(\eta,\tau) = \theta_0(\eta) + e^{-\gamma\tau}H(\eta), \\ &\phi(\eta,\tau) = \phi_0(\eta) + e^{-\gamma\tau}M(\eta) \end{aligned} \tag{27}$$

where $F(\eta)$, $H(\eta)$ and $M(\eta)$ are small relative to $f_0(\eta)$, $\theta_0(\eta)$, $\phi_0(\eta)$ and γ is small eigenvalue that will be calculated.

Substituting Eq. (27) into Eqs. (23)–(26), we get the following:

$$\frac{\partial^3 F}{\partial \eta^3} + f_0\frac{\partial^2 F}{\partial \eta^2} + Ff_0'' + (\gamma - 2f_0')\frac{\partial F}{\partial \eta} = 0 \tag{28}$$

$$\frac{1}{\mathrm{Pr}}\frac{\partial^2 H}{\partial \eta^2} + f_0\frac{\partial H}{\partial \eta} + F\theta_0' + Nb\theta_0'\frac{\partial M}{\partial \eta} + Nb\phi_0'\frac{\partial H}{\partial \eta} + 2Nt\theta_0'\frac{\partial H}{\partial \eta} + \gamma H = 0 \tag{29}$$

$$\frac{\partial^2 M}{\partial \eta^2} + Sc\, f_0\frac{\partial M}{\partial \eta} + Sc\, F\phi_0' + \frac{Nt}{Nb}\frac{\partial^2 H}{\partial \eta^2} + Sc\gamma M = 0 \tag{30}$$

with boundary conditions

$$\begin{aligned} &F(0) = 0, \quad \tfrac{\partial F(0)}{\partial \eta} = 0, \quad \tfrac{\partial H(0)}{\partial \eta} = 0, \quad Nb\tfrac{\partial M(0)}{\partial \eta} + Nt\tfrac{\partial H(0)}{\partial \eta} = 0 \quad \text{at } y = 0 \\ &\tfrac{\partial F(\eta)}{\partial \eta} \to 0, \quad H(\eta) \to 0, \quad M(\eta) \to 0 \quad \text{as } \eta \to \infty \end{aligned} \tag{31}$$

Following Weidman et al. [39], let $\tau = 0$ and get the final equations in the following form

$$F_0''' + f_0F_0'' + Ff_0'' + (\gamma - 2f_0')F_0' = 0 \tag{32}$$

$$\frac{1}{\mathrm{Pr}}H_0'' + f_0H_0' + F_0\theta_0' + Nb\theta_0'M_0' + Nb\phi_0'H_0' + 2Nt\theta_0'H_0' + \gamma H_0 = 0 \tag{33}$$

$$M_0'' + Scf_0M_0' + ScF_0\phi_0' + \frac{Nt}{Nb}H_0'' + Sc\gamma M_0 = 0 \tag{34}$$

subject to the boundary conditions

$$\begin{cases} F_0(0) = 0, \quad F_0'(0) = 0, \quad H_0'(0) = 0, \quad NbM_0'(0) + NtH_0'(0) = 0 \\ F_0'(\eta) \to 0, \quad H_0(\eta) \to 0, \quad M_0(\eta) \to 0 \quad \text{as } \eta \to \infty \end{cases} \tag{35}$$

To find the possible eigenvalues, we relax $F_0'(\eta) \to 0$ as $\eta \to \infty$ (see Harris et al. [41]).

Results and discussion

We have solved the system of nonlinear ordinary differential equations numerically using an efficient-bvp4c function. This method has been used successfully by many researchers [42–46]. For this method; suitable initial guess needs to be chosen. These guesses should satisfy the boundary conditions and keep the solution behavior. The appropriate value of similarity variable (η) is picked and the convergence criteria is kept to be 10^{-10}. We found dual solutions for a particular range of suction and stretching/shrinking parameter. The impact of following parameters such as the Prandtl number (Pr), Brownian motion parameter (*Nb*), thermophoresis parameter (*Nt*), stretching/shrinking parameter (λ), suction/injection parameter (*S*), Biot number (*Bi*) and Schmidt number (*Sc*) on the skin friction coefficient, the reduced Nusselt number, the velocity, temperature and concentration profiles will be discussed. Multiple regressions are carried out for the reduced Nusselt number. According to Turkyilmazoglu [52], if we are dealing with series solution (particularly Adomian Decomposition Method), then solution can be approximated without pre-entered values of governing parameters in an analytical manner. Thus, their accurate ranges can be determined by achieving the threshold up to the required accuracy, whereas when solving numerically, solution can only be obtained with pre-entered values of governing parameters. So here we have considered the following ranges of numerous parameters: Pr = [2,25], *Sc* = [2, 2500], *Nb* = [0.00000035, 0.5], *Nt* = [0.0000011, 0.5], and *Bi* = [0.1, ∞).

The effects of *Nb* and *Nt* on the reduced Nusselt number ($-\theta'(0)$) are observed with active and passive control of nanoparticles in Table 1 by keeping the value of Biot number large. It is seen that an increase of *Nb* does not give any effect on the heat transfer rate for passive control of nanoparticles because of the nanofluid revised model while in active control, the value decreases for both *Nb* and *Nt*. It means frequent collisions will occur because of rise in *Nb* and the nanoparticles will be more condensed. On the other hand, for passive control, a decreasing behavior is also seen for the reduced Nusselt number with *Nt*. It means that thermophoresis exhilarates the diffusion of nanoparticles and

Table 1
Numerical results of reduced Nusselt number when *Sc* = 10, λ = 01, Pr = 10, *Bi* = ∞ and *S* = 0.

Nb	*Nt*	$-\theta'(0)$ Active control of nanoparticles ($C = C_w$)	$-\theta'(0)$ Passive control of nanoparticles $\left(D_B\frac{\partial C}{\partial y} + \frac{D_T}{T_\infty}\frac{\partial T}{\partial y} = 0\right)$
3.5E−07	1.1E−06	2.307992	2.308001
3.8E−06	1.1E−06	2.307952	2.308001
3.2E−06	1.1E−06	2.307959	2.308001
0.0001	1.1E−06	2.306842	2.308001
0.001	1.1E−06	2.296475	2.308001
3.2E−06	0.0001	2.307211	2.30777
3.2E−06	0.001	2.300415	2.305665
0.1	0.1	0.952377	2.076154
0.2	0.1	0.505581	2.076154
0.3	0.1	0.252156	2.076154
0.4	0.1	0.119406	2.076154
0.1	0.2	0.693174	1.851727
0.1	0.3	0.520079	1.639971
0.1	0.4	0.402581	1.445847

Table 2
Comparison of $-\theta'(0)$ values when $Nb = Nt = S = 0$, $\lambda = 1$ and $Bi = 1000$.

Pr	$-\theta'(0)$ Present values	$-\theta'(0)$ Wang [54]	$-\theta'(0)$ Makinde and Aziz [9]
0.07	0.06562	0.0656	0.0656
0.2	0.16906	0.1691	0.1691
0.7	0.45371	0.4539	0.4539
2	0.91053	0.9114	0.9114
7	1.89182	1.8954	1.8954
20	3.35269	3.3539	3.3539

subsequently increases the thermal boundary layer thickness. That's why, the heat transfer rate is reducing. Further, to make a comparison of variation of the reduced Nusselt number, the numeric values of the reduced Nusselt number are calculated when a constant concentration of the nanoparticles and passive control of nanoparticles on the wall are adopted. Table 2 shows the comparison with published results when we replace convective boundary condition $\theta'(0) = -Bi[1-\theta(0)]$ with normal one $\theta(0) = 1$ as for $Bi \gg 1$, $\theta(0) = 1$. A decent agreement is established between the new and published results. It is also observed that with the increase of Prandtl number, the reduced Nusselt number increases. In Table 3, again we have seen the variation of the reduced Nusselt number (with active and passive control of nanoparticles) for numerous values of the Brownian motion and thermophoresis parameters by keeping the other parameters values fixed. In the first section of Table 3, we compared the present numeric values with Makinde and Aziz [9]. It is seen that Brownian motion contributes in heat transfer rate for active control of nanoparticles but show negligible impact for passive control of nanoparticles. In the second section of Table 3, we calculated the numeric values of reduced Nusselt number by using more appropriate values of governing parameters particularly Pr, *Sc*, *Nb* and *Nt*. The thermophoresis part in the rate of heat transfer is minimal and it is towards the declining trend. By observing numeric values of Tables 1 and 3, one can easily compute numerically to validate these results.

Figs. 2-10 represent the impact of different parameters on the skin-friction coefficient and the local Nusselt number. Fig. 2 shows the monotonic increase in the skin friction coefficient with an increase in suction parameter while having dual solutions up to certain ranges of stretching/shrinking parameter that are given as $\lambda_c = -1.1026$, -1.3226 and -1.5625 for $S = 2.2$, 2.3 and 2.5, respectively. It is important to mention that we can get dual solutions only for $\lambda > \lambda_c$ but the single solution and no solution for $\lambda = \lambda_c$ and $\lambda < \lambda_c$, respectively. In this

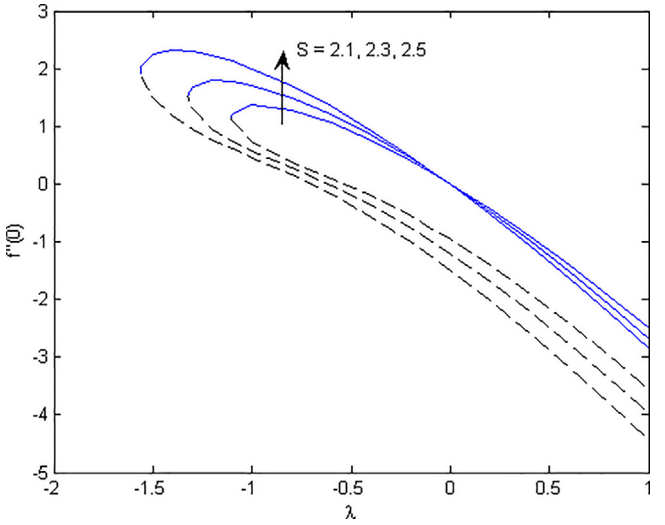

Fig. 2. Variation of the skin friction coefficient for various values of mass flux parameter.

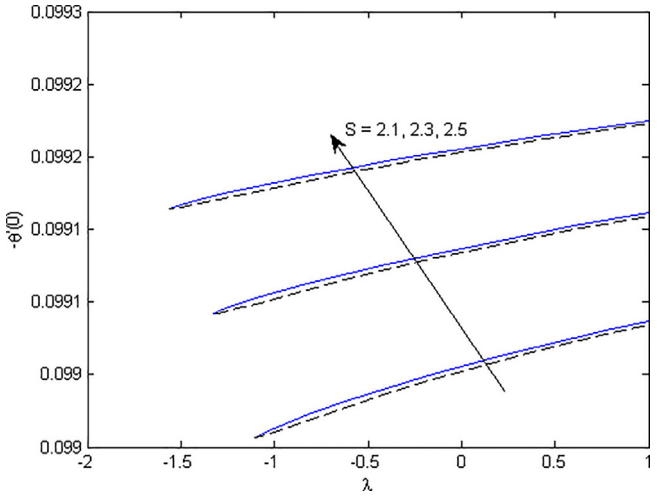

Fig. 3. Variation of the reduced Nusselt number for various values of mass flux parameter.

Table 3
The variation of reduced Nusselt number $-\theta'(0)$.

	Pr = 10, *Sc* = 10, λ = 01, *S* = 0, and *Bi* = 0.1					
	Active control of nanoparticles (Makinde and Aziz [9])			Passive control of nanoparticles (Present)		
Nb	*Nt* = 0.1	*Nt* = 0.2	*Nt* = 0.3	*Nt* = 0.1	*Nt* = 0.2	*Nt* = 0.3
0.1	0.0929	0.0927	0.0925	0.095830	0.095813	0.095796
0.2	0.0873	0.0868	0.0861	0.095830	0.095813	0.095796
0.3	0.0769	0.0751	0.0729	0.095830	0.095813	0.095796
	Pr = 7.2, *Sc* = 2500, λ = −1, *S* = 2.5, and *Bi* = 0.5. Passive control of nanoparticles					
Nb	*Nt* = 1.1E−06	*Nt* = 0.0001	*Nt* = 0.001	*Nt* = 0.01	*Nt* = 0.1	*Nt* = 0.2
3.5E−07	0.486209	0.486208	0.486207	0.486195	0.486074	0.485936
3.8E−06	0.486209	0.486208	0.486207	0.486195	0.486074	0.485936
3.2E−06	0.486209	0.486208	0.486207	0.486195	0.486074	0.485936
0.0001	0.486209	0.486208	0.486207	0.486195	0.486074	0.485936
0.01	0.486209	0.486208	0.486207	0.486195	0.486074	0.485936
0.1	0.486209	0.486208	0.486207	0.486195	0.486074	0.485936
0.2	0.486209	0.486208	0.486207	0.486195	0.486074	0.485936

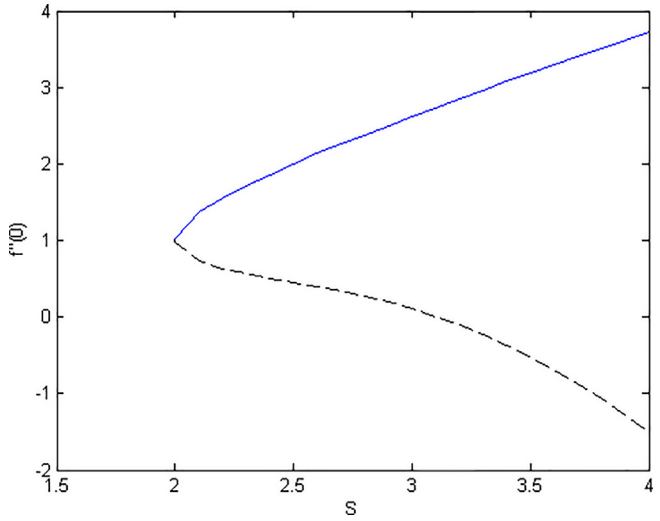

Fig. 4. Variation of the skin friction coefficient against S when $\lambda = -1$.

situation, we have to solve the full Navier-Stokes equation and energy equation. Here λ_c is the critical value. In the Figs. 2 and 3, we can observe that dual solution exists for all positive values of λ (stretching) and range of critical value also increases with increase in suction parameters. It means suction increases the range of similarity solution of Eqs. (9)–(12), namely it delays the boundary layer separation. Physically, an increase in the skin friction coefficient leads to the increase in the velocity gradient at the boundary due to increase in the shear stress at the surface. Similarly, suction parameter increases the heat transfer rate on the surface for dual solutions with an increase in the suction parameter that can be seen in Fig. 3. This is due to an increase in the surface shear stress as suction boost the penetration of the fluid.

Variations in the skin friction coefficient and the local Nusselt number against the suction parameter for the shrinking sheet are seen in Figs. 4 and 5. The critical value of the suction parameter is $S_c = 1.9998$. Here the upper branch solution is higher for $f''(0)$ and $-\theta'(0)$ as compared to the lower branch solution. Figs. 6 and 7 depict the impact of Nt and Nb. It is seen that a decrease occurs in heat transfer rate for Nt and remains same for Nb. Influence of the Brownian motion on the local Nusselt number becomes negligible due to zero nanoparticle flux on the surface. It means the contribution of Brownian motion to thermal energy equation tends to zero. This behavior is different when author actively controlled the nanoparticle fraction on the boundary. Effect of Schmidt number on the local Nusselt

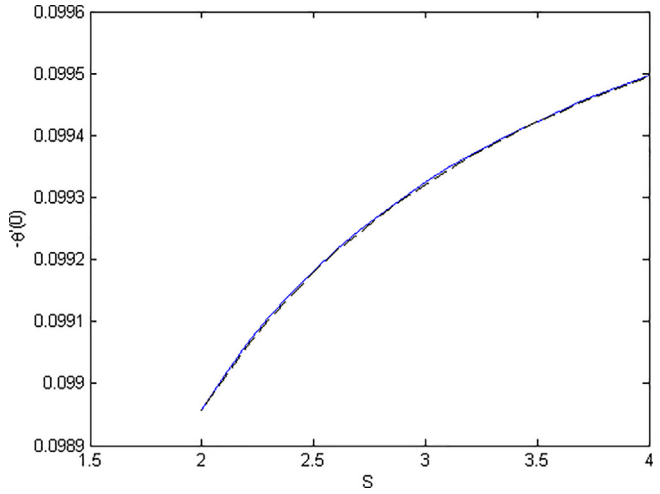

Fig. 5. Variation of the reduced Nusselt number against S when $\lambda = -1$.

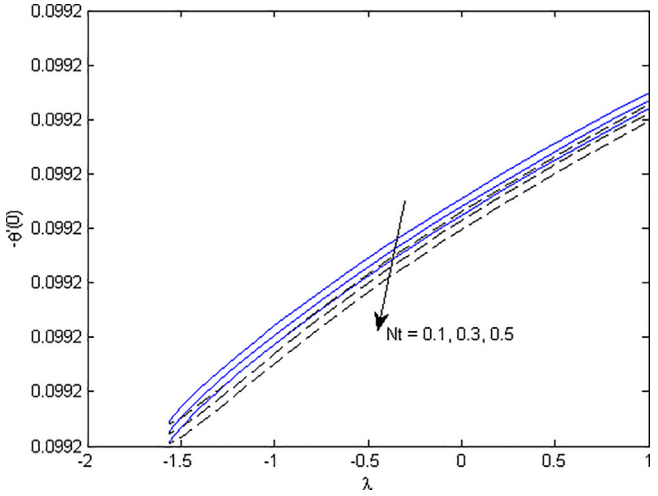

Fig. 6. Variation of the reduced Nusselt number for various values of Nt when $S = 2.5$.

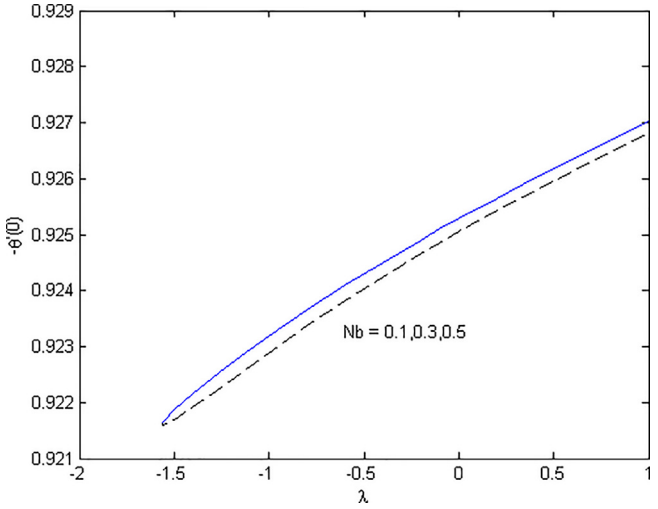

Fig. 7. Variation of the reduced Nusselt number for various values of Nb when $S = 2.5$.

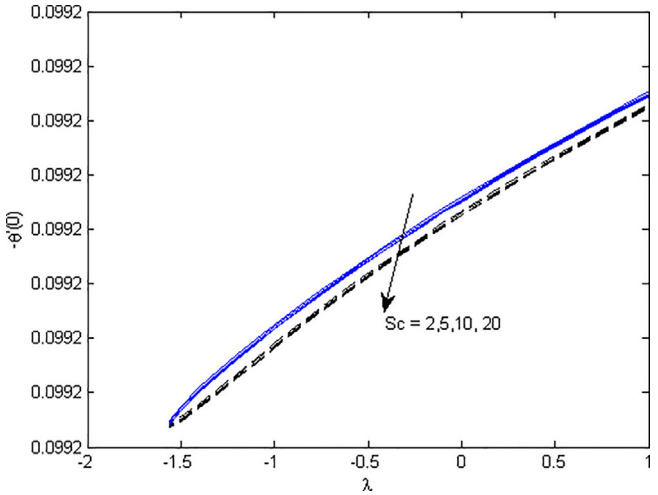

Fig. 8. Variation of the reduced Nusselt number for various values of Sc when $S = 2.5$.

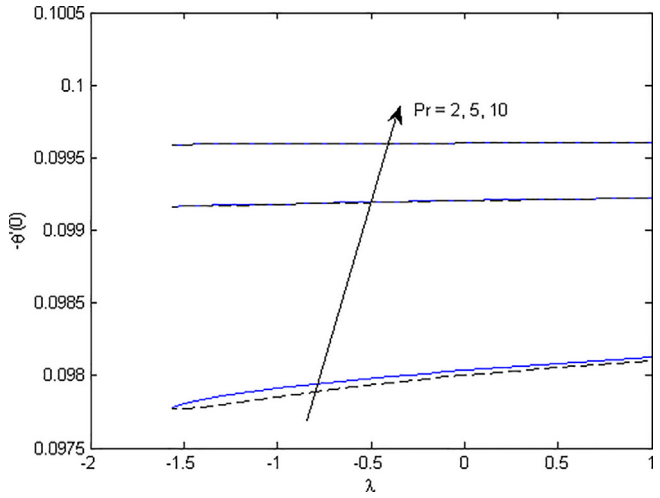

Fig. 9. Variation of the reduced Nusselt number for various values of Pr when $S = 2.5$.

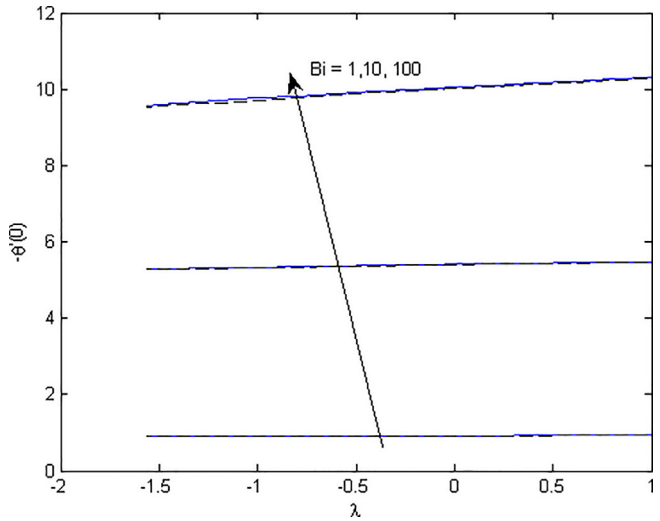

Fig. 10. Variation of the reduced Nusselt number for various values of *Bi* when $S = 2.5$.

number is seen in Fig. 8. It is seen that Schmidt number does not leave a prominent effect on the heat transfer rate although it starts decreasing with the increase of Schmidt number and the first solution has higher values as compared to the second solution. Since for higher values of *Sc*, the change in the reduced Nusselt number is very minimal. Thus the momentum diffusivity will be playing a major role in temperature and heat transfer rate (the reduced Nusselt number). It means that the minor role is played by Brownian diffusion as energy changes primarily due to the fluid motion. Fig. 9 depicts the impact of Pr on the heat transfer rate. Being proportional to the initial slope, it starts increasing for higher values of Prandtl number. Further, for higher values of the Prandtl number, thermal boundary layer becomes thinner. Subsequently, temperature gradient increases. Since Pr is the ratio of momentum diffusivity to thermal diffusion, so higher values of Prandtl number means, change in the heat transfer mainly coming from momentum diffusion. Whereas Fig. 10 illustrates the influence of Biot number on the local Nusselt number. Because of the heated surface, a strong convection occurs, and it increases the heat transfer rate deeper with an increase of Biot number/convective parameter. It is worth mentioning that one should not get confused with the Biot number and the Nusselt number as both belong to the same group of physical parameters. Basically, the Nusselt number is used to describe the heat

Table 4
Smallest eigenvalues γ at numerous values of λ.

S	λ	First solution	Second solution
0	0.5	0.2005	−0.1233
0	0.3	0.1564	−0.1021
	0.1	0.1085	−0.0771
2.1	−1	0.4	−0.3359
2.3	−1	0.7417	−0.5382
2.5	−1	1.0254	−0.6547

flux from a solid surface to a fluid while the Biot number is used to illustrate the heat transfer resistance inside a solid body.

Table 4 is presented for the results of stability analysis. We calculated the smallest eigenvalues for both stretching and shrinking sheet. For the second solution (lower branch), we got negative eigenvalues and for the first solution (upper branch), got positive eigenvalues, so it confirms that the first solution is stable and physically realizable, whereas the second solution is unstable. Note that if the smallest eigenvalue is negative, then it means there is an initial growth of disturbances, and if the smallest eigenvalue is positive, then there is an initial decay. Thus the first solution is stable to self-similar disturbances as compared to the second solution. The turning behavior of eigenvalue from positive to negative can be observed graphically. For this purpose, we draw a graph of the skin friction coefficient against suction parameter. In this graph, a transition from upper branch to lower branch occurs at $S = Sc = 1.9998$ as shown in Fig. 4. Further, to validate our argument on stability analysis, we developed a graph of smallest eigenvalues against stretching/shrinking sheet with suction effect as depicted in Fig. 11. Clearly it can be observed that smallest eigenvalue approaches to zero and make a transition from positive to negative at $\lambda = \lambda_c = -1.5625$ for $S = 2.5$. The positive eigenvalues that came out for the first solution (upper branch) are displayed as stable solution and the negative eigenvalues that we got for the second solution (lower branch) are considered as unstable solution (see Fig. 11).

The reduced Nusselt number estimation

The linear and quadratic regressions are carried out (see Nield and Kuznetsov [53]), to estimate the value of the reduced Nusselt number, which incorporates the impact of *Nb* and *Nt*. The following are the correlations for linear and quadratic regressions:

$$Nu_{est} = Nu_r + C_b Nb + C_t Nt \tag{36}$$

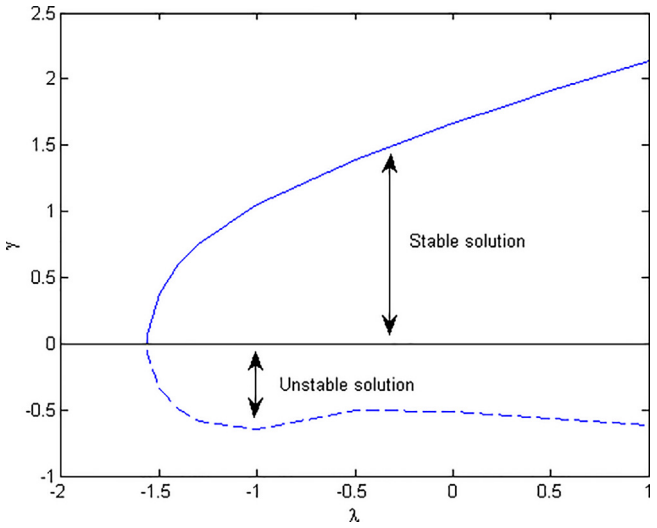

Fig. 11. The graph of smallest eigenvalues γ as a function of λ when $S = 2.5$.

Table 5
Linear regression coefficients with Adjusted R^2 and maximum relative error when $S = 2.5$, $\lambda = 0.5$ and $Bi = 1$.

Pr	Sc	Nu_r	C_b	C_t	Adjusted R^2	ε
1	10	0.721984	0.000000	−0.02683	0.999889	9.84E−05
10	10	0.961843	0.000000	−0.00379	0.99978	1.45E−05
25	10	0.984306	0.000000	−0.00091	0.999904	2.25E−06
10	20	0.961873	0.000000	−0.00518	0.999642	2.56E−05
10	100	0.961935	0.000000	−0.00734	0.999362	4.88E−05

$$Nu_{est} = Nu_r + C_bNb + C_tNt + C_{bb}Nb^2 + C_{tt}Nt^2 + C_{bt}NbNt \quad (37)$$

where C_b, C_t, C_{bb}, C_{tt}, and C_{bt} represent the coefficients of linear and quadratic regressions, respectively. For different values of the Prandtl number and the Schmidt number, the value of the reduced Nusselt number is estimated for 30 sets of values of *Nb* and *Nt* in the range of [0.1, 0.5]. The yielded regression equations are valid for *Nb* and *Nt* in the range of [0, 0.5]. Table 5 represents the linear regression coefficients at dissimilar values of the Prandtl number, and Schmidt number, whereas Table 6 is made for quadratic regression coefficients. Adjusted R^2 and maximum relative absolute error are also calculated for both regressions as shown in Tables 5 and 6. The yielded correlation of multiple linear and quadratic regressions is given below when Pr and $Sc = 10$.

$$Nu_{est} = 0.961843 + 0.000000Nb - 0.00379Nt \quad (38)$$

$$Nu_{est} = 0.961799 + 0.00000Nb - 0.00347Nt + 0.00000Nb^2 - 0.00054Nt^2 + 0.00000NbNt \quad (39)$$

From the above expression, it can be noticed that the impact of the Brownian motion parameter on the reduced Nusselt number is negligible. This is due to the nanofluid revised model. These results coincide with the graphical results in Fig. 7 and numerical results in Tables 1 and 3. Similarly, the heat transfer rate decreases for thermophoresis parameter. This behavior coincides with the graphical result presented in Fig. 6 and numerical results in Tables 1 and 3. Above correlation is made for stretching sheet. Further, to explore the impact of Brownian motion and thermophoresis on heat transfer rate, linear regressions are carried out for shrinking sheet. This time Prandtl number is selected according to the base fluid as depicted in Tables 7 and 8. Since Schmidt number should be selected higher for nanofluid, we tried to estimate the correlation for maximum value of *Sc* that is 1000. Since for most practical purpose, linear regression is adequate (see Nield and Kuznetsov [53]), so here for shrinking sheet, we limit our regression to only linear regression. From Tables 7 and 8, estimated values of the reduced Nusselt number for various values of Prandtl and Schmidt numbers can be observed. Further, it is observed that for various base fluids, rate of heat transfer is different and it increases accordingly as Prandtl number is increased. The role of the Brownian motion in heat transfer also become zero for shrinking sheet due to passive control of nanoparticles. According to Table 8 results, the role of Schmidt number becomes minimal with rise in its values in heat transfer rate accordingly. As higher value of Schmidt number we consider, in the same way its impact decreases because of a very minor role of Brownian diffusion. The contribution of thermophoresis, Brownian motion, Schmidt number and

Table 7
Linear regression coefficients with Adjusted R^2 and maximum relative error when $S = 2.5$, $\lambda = -1$ and $Bi = 1$.

Pr	Sc	Nu_r	C_b	C_t	Adjusted R^2	ε
1	10	0.693555	0.000000	−0.03211	0.99988	1.27E−04
3.97	10	0.905607	0.000000	−0.01301	0.999667	6.60E−05
6.8	10	0.943363	0.000000	−0.00689	0.999704	3.15E−05
14.2	10	0.972334	0.000000	−0.00239	0.999818	8.26E−06
21	10	0.981181	0.000000	−0.00127	0.999877	3.56E−06

Table 8
Linear regression coefficients with Adjusted R^2 and maximum relative error when $S = 2.5$, $\lambda = -1$ and $Bi = 1$.

Sc	Pr	Nu_r	C_b	C_t	Adjusted R^2	ε
10	6.8	0.943363	0.000000	−0.00689	0.999704	3.15E−05
50	6.8	0.943457	0.000000	−0.01045	0.999422	6.74E−05
100	6.8	0.943481	0.000000	−0.01118	0.999349	7.67E−05
1000	6.8	0.943508	0.000000	−0.01193	0.999265	8.71E−05

Prandtl number in heat transfer rate tally with graphical results depicted in Figs. 6–9. Since from Tables 1, 3 and 5–8 and Figs. 6–8, it is evident that the heat transfer rate remains stagnant for the Brownian motion and *Nt* contribute at minimum level, for $Sc > 1$, Brownian diffusion role is also minimum. Further, nanofluid flow is being disturbed with deformation of sheet, so overall, the role of *Nb* and *Nt* is small. Hence, in our point of view, the values of *Nb* and *Nt* should be chosen to be small as majority of heat transfer is driven by fluid motion.

This section containing Figs. 12 to 18 discoursed the impact of numerous parameters on convective boundary layer and nanoparticle volume fraction, and all graphical results asymptotically satisfy far field boundary conditions. The impact of the Brownian motion on thermal boundary layer and nanoparticle volume fraction is shown in Figs. 12 and 13. Zero effect is seen for temperature distribution against the stretching/shrinking sheet that is consistent with Fig. 7 drawn for the local Nusselt number, whereas a decreasing behavior is seen for nanoparticle distribution in Fig. 13 either sheet is stretching or shrinking. Interestingly nanoparticle volume fraction first overshoots and then gradually decreases as the wall is approached because of the passive control of nanoparticles on the wall. The same behavior is observed for volume fraction at numerous values of *Sc* but we do not include here due to space limitation. The thermophoresis parameter has a minimal increasing effect on temperature profile for both stretching/shrinking sheet as depicted in Fig. 14. Basically it increases the thermal boundary layer thickness so subsequently heat transfer rate should decrease, and it is evident in Fig. 6. Moreover, nanoparticle volume fraction increases with significant effect as we increase *Nt* for both cases of the sheet but did not include figures due to space limitation. Fig. 15 reveals that the temperature distribution increases with the increase of *Sc* but its effects are only perceptible near to the sheet. So it means, an increase in temperature profile is to decrease the heat transfer rate that is obvious in Fig. 8. Figs. 16 and 17 demonstrate the influence of *Bi* on the temperature and concentration profiles. Biot number increases the temperature and nanoparticle concentration distributions in consort with

Table 6
Quadratic regression coefficients with Adjusted R^2 and maximum relative error when $S = 2.5$, $\lambda = 0.5$ and $Bi = 1$.

Pr	Sc	Nu_r	C_b	C_t	C_{bb}	C_{tt}	C_{bt}	Adjusted R^2	ε
1	10	0.721765	0.00000	−0.02521	0.00000	−0.00269	0.00000	1	9.23E−07
10	10	0.961799	0.00000	−0.00347	0.00000	−0.00054	0.00000	1	3.28E−07
25	10	0.984299	0.00000	−0.00086	0.00000	−8.6E−05	0.00000	1	2.64E−08
10	20	0.961797	0.00000	−0.00462	0.00000	−0.00094	0.00000	1	5.60E−07
10	100	0.961791	0.00000	−0.00628	0.00000	−0.00177	0.00000	1	1.43E−06

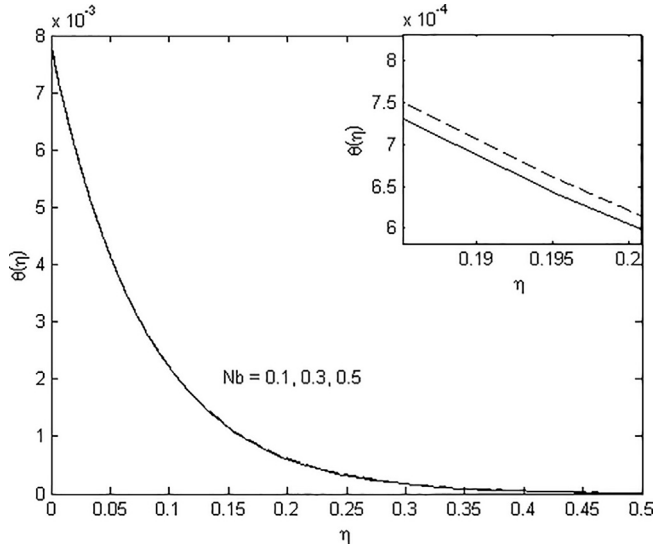

Fig. 12. Variation of temperature profile for *Nb* when $\lambda = 0.5/-1$.

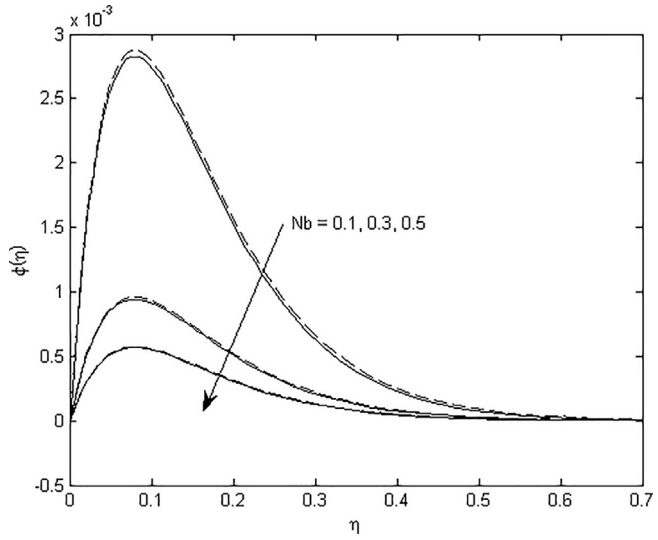

Fig. 13. Variation of nanoparticle distribution for *Nb* when $\lambda = 0.5/-1$.

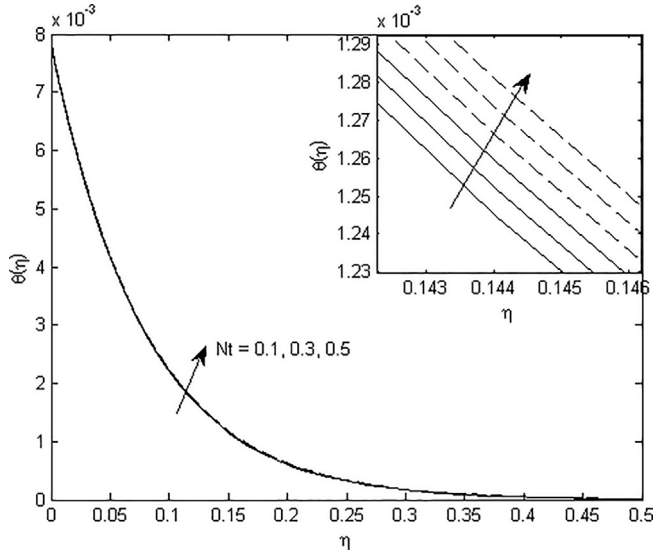

Fig. 14. Variation of temperature profile for *Nt* when $\lambda = 0.5/-1$.

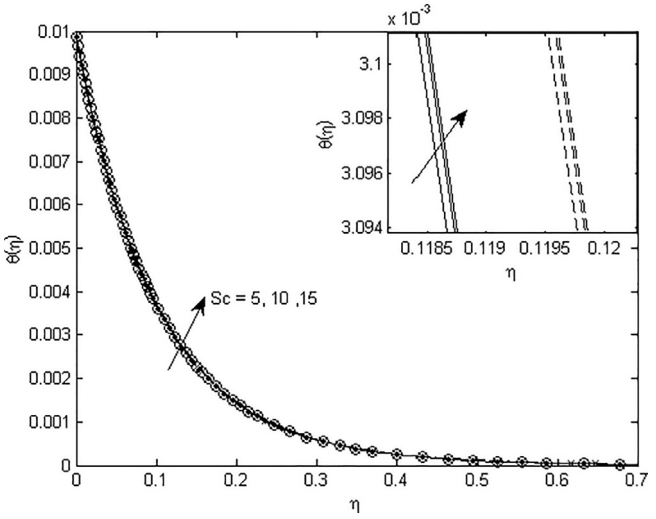

Fig. 15. Variation of temperature profile for *Sc* when $\lambda = -1$.

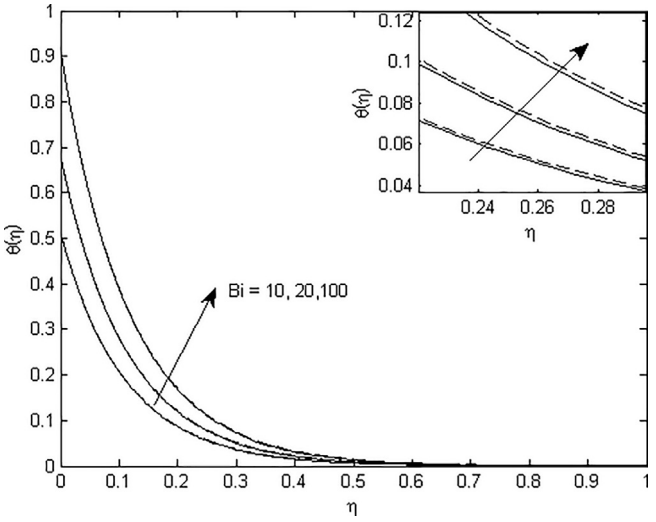

Fig. 16. Variation of temperature profile for *Bi* when $\lambda = -1$.

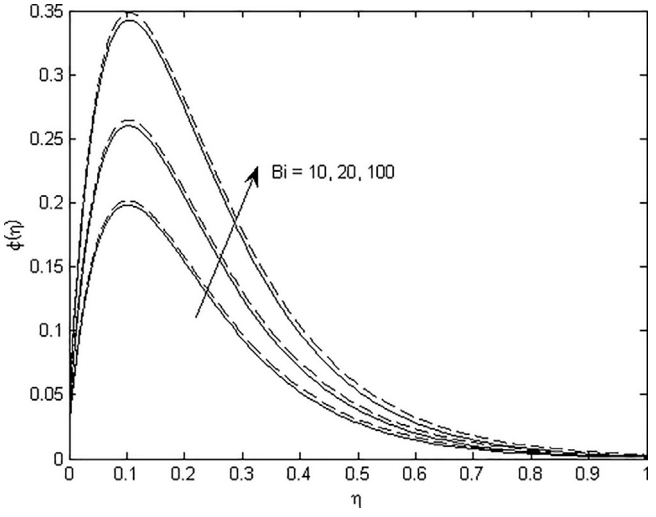

Fig. 17. Variation of nanoparticle distribution for *Bi* when $\lambda = -1$.

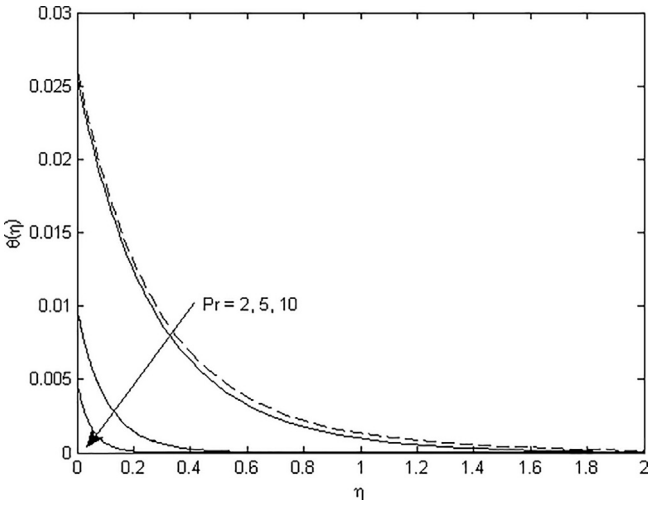

Fig. 18. Variation of temperature profile for Pr when $\lambda = -1$.

boundary layer thickness. In reality, the increase in Biot number increases the penetration depth. Further, Fig. 17 depicts the flipping behavior as the nanoparticle flux at the surface is suppressed. The increase in Prandtl number decreases the thermal boundary layer thickness as revealed in Fig. 18. This result is consistent with Fig. 9 where heat transfer rate increases with increase in Pr.

Lastly, the flow pattern is analyzed in Fig. 19(a)–(h). In these figures we draw the streamlines to observe the flow pattern. For the impermeable case ($S = 0$), flow behaves the same as for the stagnation point flow but for the second solution, it is divided into two regions, the first region behaves the same as for the first solution but the second region shows that the flow rotates in reverse direction. It is observed that the streamline contracts with the increase of the suction parameter. As a result, density increases that causes an increase in fluid velocity.

Conclusions

We studied the boundary layer flow of nanofluid for a permeable stretching/shrinking sheet with convective boundary condition by controlling the nanoparticle fraction passively rather than actively on the boundaries. This is a more realistic approach. The nonlinear system of ordinary differential Eqs. (9)–(11) with a set of new boundary conditions (12) is solved with the help of bvp4c function. The validity of our calculation is shown through comparison. The stability of the outcoming solutions for stretching/shrinking sheet under the impermeable and suction effect is shown by finding the smallest eigenvalues for both solutions, and it is observed that first solution is stable and realizable. The turning point from positive to negative eigenvalues for dual solutions is explained graphically. The reduced Nusselt number is estimated for 30 sets of values of *Nb* and *Nt* using regression for both stretching and shrinking sheets and the impact of *Nb* and *Nt* is observed for heat transfer rate. The Brownian motion parameter does not bring any change in the heat transfer rate and for the temperature profile. Thus the reduced Nusselt number is almost independent of *Nb* when we imposed zero flux on the boundary using realistic approach. The values of *Nb* and *Nt* should be chosen small since in a moving liquid, energy transfer would be primarily owing to the fluid motion. The increase in the suction parameter widened the range of the stretching/shrinking parameter. Heat transfer rate is higher for higher values of the suction parameter. Temperature distribution increased with an increase in *Nt* that is consistent with the result when heat transfer rate decreased with *Nt*. Schmidt number depicted minimal decrease in the reduced Nusselt number. On the other hand, temperature distribution showed a minimal increase with *Sc* that depicted consistency with heat transfer rate. The increase in the Prandtl number showed a decrease in temperature profile, while increase occured in the heat transfer rate with Pr. The higher values of Pr indicates the change in heat transfer via fluid motion instead of thermal diffusion. The temperature distribution and heat transfer rate are higher for large values of the Biot number. The streamline contracted due to increase in the suction parameter, whereas for the impermeable case, oncoming flow behaved as a stagnation point flow.

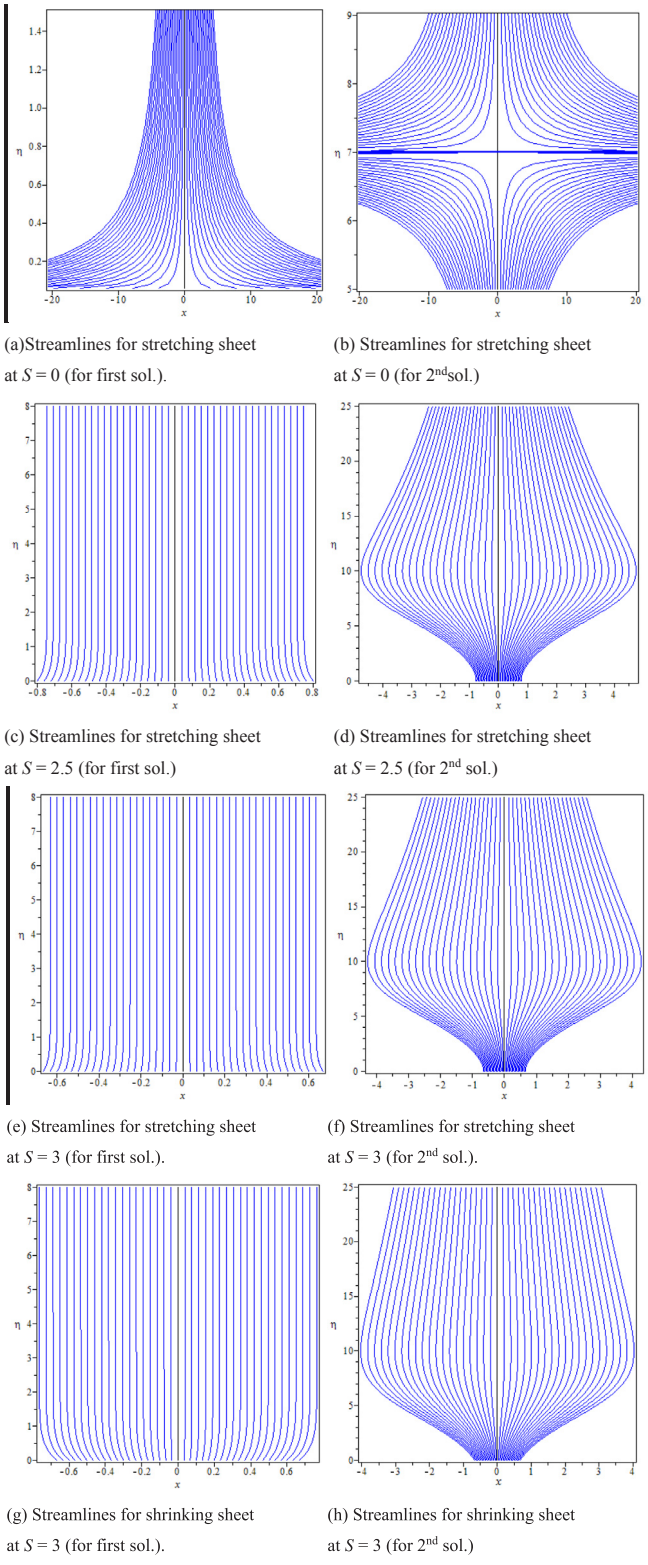

(a)Streamlines for stretching sheet at $S = 0$ (for first sol.).

(b) Streamlines for stretching sheet at $S = 0$ (for 2nd sol.)

(c) Streamlines for stretching sheet at $S = 2.5$ (for first sol.)

(d) Streamlines for stretching sheet at $S = 2.5$ (for 2nd sol.)

(e) Streamlines for stretching sheet at $S = 3$ (for first sol.).

(f) Streamlines for stretching sheet at $S = 3$ (for 2nd sol.).

(g) Streamlines for shrinking sheet at $S = 3$ (for first sol.).

(h) Streamlines for shrinking sheet at $S = 3$ (for 2nd sol.)

Fig. 19. Sketch of streamlines.

Acknowledgements

The first author is grateful to Universiti Teknologi PETRONAS for the financial support received in terms of a graduate assistantship (GA/003/A). The corresponding author would like to acknowledge the research university grant (DIP-2017-009) from the Universiti Kebangsaan Malaysia. The work of I. Pop has been supported from the grant PN-III-P4-ID-PCE-2016-0036, UEFISCDI, Romania. The authors also wish to express their thanks to the very competent Reviewers for the valuable comments and suggestions.

References

[1] Masuda H, Ebata A, Teramae K. Alteration of thermal conductivity and viscosity of liquid by dispersing ultra-fine particles. Dispersion of Al_2O_3, SiO_2 and TiO_2 ultra-fine particles. NETSU BUSSEI 1993;7(4):227–33.
[2] Das SK, Putra N, Thiesen P, Roetzel W. Temperature dependence of thermal conductivity enhancement for nanofluids. J Heat Transfer 2003;125(4):567–74.
[3] Pak BC, Cho YI. Hydrodynamic and heat transfer study of dispersed fluids with submicron metallic oxide particles. Exper Heat Transfer Int J 1998;11(2):151–70.
[4] Xuan Y, Li Q. Investigation on convective heat transfer and flow features of nanofluids. J Heat Transfer 2003;125(1):151–5.
[5] Eastman JA, Choi S, Li S, Yu W, Thompson L. Anomalously increased effective thermal conductivities of ethylene glycol-based nanofluids containing copper nanoparticles. Appl Phys Lett 2001;78(6):718–20.
[6] Mintsa HA, Roy G, Nguyen CT, Doucet D. New temperature dependent thermal conductivity data for water-based nanofluids. Int J Therm Sci 2009;48(2):363–71.
[7] Kakac S, Pramuanjaroenkij A. Review of convective heat transfer enhancement with nanofluids. Int J Heat Mass Transfer 2009;52(13):3187–96.
[8] Khan W, Pop I. Boundary-layer flow of a nanofluid past a stretching sheet. Int J Heat Mass Transfer 2010;53(11):2477–83.
[9] Makinde O, Aziz A. Boundary layer flow of a nanofluid past a stretching sheet with a convective boundary condition. Int J Therm Sci 2011;50(7):1326–32.
[10] Turkyilmazoglu M. Algebraic solutions of flow and heat for some nanofluids over deformable and permeable surfaces. Int J Numer Methods Heat Fluid Flow 2017;27(10):2259–67.
[11] Khan SU, Shehzad SA, Rauf A, Ali N. Mixed convection flow of couple stress nanofluid over oscillatory stretching sheet with heat absorption/generation effects. Results Phys 2018;8:1223–31.
[12] Das SK, Choi SUS, Yu W, Pradeep T. Nanofluids: science and technology. New York: John Wiley & Sons; 2007.
[13] Vafai K. Porous media: applications in biological systems and biotechnology. CRC Press; 2010.
[14] Michaelides EE. Nanofluidics: thermodynamic and transport properties. Cham, Switzerland: Springer International Publishing; 2014.
[15] Nield D, Bejan A. Convection in porous media. 4th ed. New York, NY: Springer; 2013.
[16] Shenoy A, Sheremet M, Pop I. Convective flow and heat transfer from wavy surfaces: viscous fluids, porous media, and nanofluids. CRC Press; 2016.
[17] Buongiorno J, et al. A benchmark study on the thermal conductivity of nanofluids. J Appl Phys 2009;106:1–14.
[18] Kakaç S, Pramuanjaroenkij A. Review of convective heat transfer enhancement with nanofluids. Int J Heat Mass Transfer 2009;52:3187–96.
[19] Wong KFV, Leon OD. Applications of nanofluids: current and future. Adv Mech Eng 2010;2010:1–11.
[20] Manca O, Jaluria Y, Poulikakos D. Heat transfer in nanofluids. Adv Mech Eng 2010;2010:380826.
[21] Mahian O, Kianifar A, Kalogirou SA, Pop I, Wongwises S. A review of the applications of nanofluids in solar energy. Int. J. Heat Mass Transfer 2013;57:582–94.
[22] Sheikholeslami M, Ganji D. Nanofluid convective heat transfer using semi analytical and numerical approaches: a review. J Taiwan Inst Chem Eng 2016;65:43–77.
[23] Ganvir R, Walke P, Kriplani V. Heat transfer characteristics in nanofluid—A review. Renewable Sustainable Energy Rev 2017;75:451–60.
[24] Bahiraei M, Rahmani R, Yaghoobi A, Khodabandeh E, Mashayekhi R, Amani M. Recent research contributions concerning use of nanofluids in heat exchangers: A critical review. Appl Thermal Eng 2018;133:137–59.
[25] Rao SS, Srivastava A. Whole field measurements to understand the effect of nanoparticle concentration on heat transfer rates in a differentially-heated fluid layer. Exp Therm Fluid Sci 2018;92:326–45.
[26] Buongiorno J. Convective transport in nanofluids. J Heat Transfer 2006;128(3):240–50.
[27] Kuznetsov AV, Nield D. The Cheng-Minkowycz problem for natural convective boundary layer flow in a porous medium saturated by a nanofluid: a revised model. Int J Heat Mass Transfer 2013;65:682–5.
[28] Nield D, Kuznetsov AV. Thermal instability in a porous medium layer saturated by a nanofluid: a revised model. Int J Heat Mass Transfer 2014;68:211–4.
[29] Nield D, Kuznetsov AV. The onset of convection in a horizontal nanofluid layer of finite depth: a revised model. Int J Heat Mass Transfer 2014;77:915–8.
[30] Kuznetsov AV, Nield D. Natural convective boundary-layer flow of a nanofluid past a vertical plate: a revised model. Int J Therm Sci 2014;77:126–9.
[31] Yadav D, Agrawal G, Lee J. Thermal instability in a rotating nanofluid layer: a revised model. Ain Shams Eng J 2015;7:431–40.
[32] Yadav D, Lee D, Cho HH, Lee J. The onset of double-diffusive nanofluid convection in a rotating porous medium layer with thermal conductivity and viscosity variation: a revised model. J Porous Media 2016;19:31–46.
[33] Rana G, Chand R. Stability analysis of double-diffusive convection of Rivlin-Ericksen elastico-viscous nanofluid saturating a porous medium: a revised model. Forsch Ingenieurwes 2015;79:87–95.
[34] Jahan S, Sakidin H, Nazar R, Pop I. Boundary layer flow of nanofluid over a moving surface in a flowing fluid using revised model with stability analysis. Int J Mech Sci 2017;131:1073–81.
[35] Uddin I, Khan MA, Ullah S, Islam S, Israr M, Hussain F. Characteristics of buoyancy force on stagnation point flow with magneto-nanoparticles and zero mass flux condition. Results Phys 2018;8:160–8.
[36] Aleng NL, Bachok N. Dual solutions of exponentially stretched/shrinked flows of nanofluids. J Nanofluids 2018;7(1):195–202.
[37] Turkyilmazoglu M. Analytical solutions to mixed convection MHD fluid flow induced by a nonlinearly deforming permeable surface. Commun Nonlinear Sci Numer Simul 2018.
[38] Merkin J. On dual solutions occurring in mixed convection in a porous medium. J Eng Math 1986;20(2):171–9.
[39] Weidman P, Kubitschek D, Davis A. The effect of transpiration on self-similar boundary layer flow over moving surfaces. Int J Eng Sci 2006;44(11):730–7.
[40] Merrill K, Beauchesne M, Previte J, Paullet J, Weidman P. Final steady flow near a stagnation point on a vertical surface in a porous medium. Int J Heat Mass Transfer 2006;49(23):4681–6.
[41] Harris S, Ingham D, Pop I. Mixed convection boundary-layer flow near the stagnation point on a vertical surface in a porous medium: Brinkman model with slip. Transp Porous Media 2009;77(2):267–85.
[42] Roşca AV, Pop I. Flow and heat transfer over a vertical permeable stretching/shrinking sheet with a second order slip. Int J Heat Mass Transfer 2013;60:355–64.
[43] Ishak A. Flow and heat transfer over a shrinking sheet: a stability analysis. Int J Mech Aeros Indus Mech Eng 2014;8:872–6.
[44] Nazar R, Noor A, Jafar K, Pop I. Stability analysis of three-dimensional flow and heat transfer over a permeable shrinking surface in a Cu-water nanofluid, World Academy of Engineering and Technology. Int J Math Comput Phys Elect Comput Eng 2014;8(5):780–6.
[45] Hamid RA, Nazar R, Pop I. The non-alignment stagnation-point flow towards a permeable stretching/shrinking sheet in a nanofluid using Buongiorno's model: a revised model. Zeitschrift für Naturforschung A 2016;71(1):81–9.
[46] Awaludin I, Weidman P, Ishak A. Stability analysis of stagnation-point flow over a stretching/shrinking sheet. AIP Adv 2016;6(4):045308.
[47] Rosca NC, Pop I. A numerical study of the axisymmetric rotational stagnation point flow impinging radially a permeable stretching/shrinking surface in a nanofluid. Int J Numer Meth Heat Fluid Flow 2017;27(11):2415–32.
[48] Haddad Z, Abu-Nada E, Oztop HF, Mataoui A. Natural convection in nanofluids: are the thermophoresis and Brownian motion effects significant in nanofluid heat transfer enhancement. Int J Thermal Sci 2012;57:152–62.
[49] Fang T, Zhang J. Closed-form exact solutions of MHD viscous flow over a shrinking sheet. Commun Nonlinear Sci Numer Simul 2009;14(7):2853–7.
[50] Turkyilmazoglu M. Equivalences and correspondences between the deforming body induced flow and heat in two-three dimensions. Phys Fluids 2016;28:043102.
[51] Weidman P, Sprague M. Flows induced by a plate moving normal to stagnation-point flow. Acta Mech 2011;219:219–29.
[52] Turkyilmazoglu M. Determination of the correct range of physical parameters in the approximate analytical solutions of nonlinear equations using the Adomian decomposition method. Mediterranean J Math 2016;13:4019–37.
[53] Nield D, Kuznetsov A. The Cheng-Minkowycz problem for natural convective boundary-layer flow in a porous medium saturated by a nanofluid. Int J Heat Mass Transfer 2009;52(25):5792–5.
[54] Wang C. Free convection on a vertical stretching surface. J Appl Math Mech (ZAMM) 1989;69(11):418–20.